Internal electric-field intensity distribution of a monolayer of periodically arrayed dielectric spheres

doi: 10.1103/PhysRevB.70.155107

Internal electric-field intensity distribution of a monolayer of periodically arrayed dielectric spheres

Y. Kurokawa*
Materials Engineering Laboratory National Institute for Materials Science, 1-2-1 Sengen, Tsukuba, Ibaraki 305-0047, Japan

Y. Jimba
College of Engineering, Nihon University, Koriyama, Fukushima 963-8642, Japan

H. Miyazaki
Department of Applied Physics, Tohoku University, Aramaki, Aoba, Sendai 980-8579, Japan
(Received 24 May 2004; published 21 October 2004)

Theoretical analysis is given for the internal electric-field distribution of two-dimensional periodic dielectric spheres by extending the vector Korringa-Kohn-Rostoker method. It is shown that the internal electric-field intensity distribution of the monolayer with high dielectric constant is in good agreement with that of an isolated sphere at the Mie resonance. In contrast, the field distribution of the monolayer with low dielectric constant is complicated and strongly influenced by the interaction between spheres. Our results show that the internal electric field of the monolayer presents important information about the origin of each eigenstate.

DOI: 10.1103/PhysRevB.70.155107 PACS number(s): 42.70.Qs, 42.25.Bs, 42.79.−e

Photonic crystals (PhC's) are expected to play an important role for the development of optoelectronic technology, because PhC's have attractive properties for application. These properties are brought about by the photonic band structure of PhC's due to the periodicity of dielectric constant. PhC's with large photonic band gaps (PBG's) have particularly attracted much interest,[1–3] since they can be used for control of the spontaneous emission of atomic systems and waveguides. In addition, it is reported that the photonic band dispersion also exhibits interesting optical properties, for example, the superprism effect.[4] To fully utilize these properties, we need to understand the origin of the photonic band structure.

A typical example of PhC's is the two-dimensional (2D) periodic dielectric spheres. Since the monolayer is an important system for the physical understanding of the origin of the photonic band structure, those with high or low dielectric constant have been widely investigated.[5–11] There are two widely used concepts for the understanding of the band structure.[12] One is the tight-binding description, and the other is the nearly-free-photon approximation. In the case of dielectric spheres, the tight-binding approximation is suitable for describing the eigenstate due to the Mie resonance states.[13] In contrast, the nearly-free-photon approximation is based on the folding of the dispersion of free photon in the Brillouin zone.[14]

We can discuss the origin of the eigenstate of each band by the electric-field intensity distribution near the crystal, because we can obtain the characteristic field intensity distribution unique to each eigenstate when the eigenstate is excited by the incident light. The near-field intensity, i.e., the electric-field intensity distribution just outside the monolayer, has been studied[6] by the vector Korringa-Kohn-Rostoker (KKR) method[15,16] with very high accuracy and faster convergence. We expect that the internal electric-field intensity distribution of the monolayer gives more detailed information than the near-field intensity distribution. So far, however, the field distribution inside the monolayer has not yet been studied.

In this paper, we extend the vector KKR method to calculate the internal electric field of the monolayer. We examine numerically the internal electric-field intensity distribution of the monolayer and discuss the origin of each eigenstate. It is shown that detailed and fruitful information can be obtained on the origin of each band by investigating the internal electric field of the monolayer with various dielectric constants.

We deal with a monolayer of periodically arrayed dielectric spheres as shown in Fig. 1. The radius and lattice constant of spheres are, respectively, denoted by a and d. The dielectric constant of spheres is denoted by ε. Spheres are arranged in the xy plane to form a triangular lattice. We take the origin of coordinates as the center of one of the spheres. The plane electromagnetic wave $E_i^0(\mathbf{r})$ of the wave vector $\mathbf{k}_0=(\mathbf{k}_\parallel,\Gamma_0^+)$ and amplitude E_i^0 is incident upward from below:

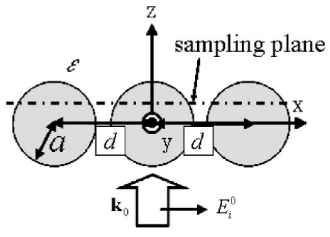

FIG. 1. Two-dimensional periodic dielectric spheres of radius a and lattice constant d. The dielectric constant of spheres is ε. The origin of coordinates is chosen at the center of one of the spheres. The plane electromagnetic wave of the wave vector $\mathbf{k}_0$ and amplitude E_i^0 is incident upward from below. The height of the sampling plane is $0.4a$. The sampling plane is shown by the broken line.

$$E_i^0(\mathbf{r}) = E_i^0 \exp(i\mathbf{k}_0 \cdot \mathbf{r}), \tag{1}$$

where i represents the Cartesian component, and $\mathbf{k}_\parallel = (k_x, k_y)$ is the in-plane component of $\mathbf{k}_0$. $\Gamma_0^+ = +\sqrt{\mathbf{k}_0^2 - \mathbf{k}_\parallel^2}$ is the z component of $\mathbf{k}_0$ and is given from the energy conservation law. From the vector KKR formalism,[16] the scattered field $E_i^s(\mathbf{r})$ is expressed by

$$E_i^s(\mathbf{r}) = \sum_{j,j_1} \int_{r_1<a} \int_{r_2<a} d\mathbf{r}_1 d\mathbf{r}_2 g_{i,j_1}(\mathbf{r},\mathbf{r}_1) T_{j_1,j}(\mathbf{r}_1,\mathbf{r}_2) E_j^0(\mathbf{r}_2), \tag{2}$$

where

$$g_{i,j}(\mathbf{r},\mathbf{r}') = \left(\delta_{i,j} + \frac{1}{k_0^2} \frac{\partial}{\partial x_i} \frac{\partial}{\partial x_j} \right) G(\mathbf{r},\mathbf{r}').$$

$G(\mathbf{r},\mathbf{r}')$ is the Green function, satisfying $(\nabla^2 + k_0^2) G(\mathbf{r},\mathbf{r}') = \delta(\mathbf{r}-\mathbf{r}')$, and $k_0 = |\mathbf{k}_0|$. $E_i^s(\mathbf{r})$ must satisfy periodic boundary conditions, because the dielectric constant is periodic. Therefore, $G(\mathbf{r},\mathbf{r}')$ fulfills Bloch's theorem. $T_{i,j}(\mathbf{r},\mathbf{r}')$ represents the multiple scattering between spheres.

The electric field outside the spheres is expanded by spherical waves:

$$\begin{aligned} E_i^{s(0)}(\mathbf{r}) + E_i^{s(1)}(\mathbf{r}) + E_i^0(\mathbf{r}) = & -ik_0 \mathbf{Y}^t(\hat{\mathbf{r}}) \underline{\mathbf{h}}^{(1)}(k_0 r) \sum_{\beta,\beta'} \underline{\mathbf{P}}_i^\beta \underline{\mathbf{t}}^\beta \{[\underline{\mathbf{I}} \\ & - \underline{\boldsymbol{\gamma}}(\mathbf{k}_\parallel)\underline{\mathbf{t}}]^{-1}\}^{\beta\beta'} \boldsymbol{\alpha}^{\beta'}(0) \\ & + \mathbf{Y}^t(\hat{\mathbf{r}}) \underline{\mathbf{j}}(k_0 r) \sum_{\beta,\beta'} \underline{\mathbf{P}}_i^\beta \{[\underline{\mathbf{I}} \\ & - \underline{\boldsymbol{\gamma}}(\mathbf{k}_\parallel)\underline{\mathbf{t}}]^{-1}\}^{\beta\beta'} \boldsymbol{\alpha}^{\beta'}(0). \end{aligned} \tag{3}$$

The scattered fields $E_i^{s(0)}(\mathbf{r})$ and $E_i^{s(1)}$ from one of the spheres and other spheres are obtained by incorporating the multiple scattering between spheres. β is TE for transverse electric field and TM for transverse magnetic field. We use matrix notation with quantum numbers ℓ and m. $\underline{\mathbf{j}}(kr)$ and $\underline{\mathbf{h}}^{(1)}(kr)$ are diagonal matrices of the spherical Bessel function $j_\ell(kr)$ and the spherical Hankel function of the first kind $h_\ell^{(1)}(kr)$, respectively. $\mathbf{Y}(\hat{\mathbf{r}})$ is a column vector of the spherical harmonics. The matrix $\underline{\mathbf{P}}_i^\beta$ is the expansion coefficient of the ith component of the vector spherical waves into the sherical harmonics,[15] ℓ and ℓ' run over $\ell \geq 1$ and $\ell' \geq 0$, respectively. $\boldsymbol{\alpha}^\beta(0)$ is the column vector of the incindent light.[16] The expansion coefficient $\underline{\mathbf{t}}^\beta$ is obtained from the Mie theory.[16] The definition of $\underline{\boldsymbol{\gamma}}^{\beta\beta'}(\mathbf{k}_\parallel)$ is

$$\underline{\boldsymbol{\gamma}}^{\beta\beta'}(\mathbf{k}_\parallel) = -ik_0 \underline{\mathbf{L}} \sum_j (\underline{\mathbf{P}}_j^\beta)^+ \underline{\boldsymbol{\Gamma}}(\mathbf{k}_\parallel) \underline{\mathbf{P}}_j^{\beta'}. \tag{4}$$

Here, the matrix $\underline{\boldsymbol{\Gamma}}(\mathbf{k}_\parallel)$ is the structure factor.[17] The matrix $L_{\ell m \ell' m'} = \delta_{\ell,\ell'} \delta_{m,m'} / \{\ell(\ell+1)\}$ is defined within $\ell, \ell' \geq 1$.[16] $\underline{\mathbf{I}}$ is a unit matrix.

The electric field in the spheres is defined by

$$E_i^w(\mathbf{r}) = -ik_0 \mathbf{Y}^t(\hat{\mathbf{r}}) \underline{\mathbf{j}}(k_< r) \sum_{\beta,\beta'} \underline{\mathbf{P}}_i^\beta \underline{\mathbf{w}}^\beta \{[\underline{\mathbf{I}} - \underline{\boldsymbol{\gamma}}(\mathbf{k}_\parallel)\underline{\mathbf{t}}]^{-1}\}^{\beta\beta'} \boldsymbol{\alpha}^{\beta'}(0). \tag{5}$$

The expansion coefficient $\underline{\mathbf{w}}^\beta$ is obtained by boundary condition at the surface of the spheres:

$$w_\ell^{\mathrm{TE}} = \frac{i}{k_0} \frac{k_0 h_\ell^{(1)}(k_0 a) j_\ell'(k_0 a) - k_0 j_\ell(k_0 a) h_\ell^{(1)\prime}(k_0 a)}{k_< h_\ell^{(1)}(k_0 a) j_\ell'(k_< a) - k_0 j_\ell(k_< a) h_\ell^{(1)\prime}(k_0 a)}, \tag{6}$$

$$w_\ell^{\mathrm{TM}} = \frac{i}{k_0} \frac{k_< k_0^2 a^2 [h_\ell^{(1)\prime}(k_0 a) j_\ell(k_0 a) - h_\ell^{(1)}(k_0 a) j_\ell'(k_0 a)]}{(k_<^2 - k_0^2) a j_\ell(k_< a) h_\ell^{(1)}(k_0 a) + k_0 k_< a^2 \phi_\ell}, \tag{7}$$

where

$$\phi_\ell = k_< h_\ell^{(1)\prime}(k_0 a) j_\ell(k_< a) - k_0 h_\ell^{(1)}(k_0 a) j_\ell'(k_< a). \tag{8}$$

The prime denotes the differentiation with respect to the argument, and $k_<$ is the wave number in the spheres.

We discuss the origin of the eigenstates of the monolayer with high or low dielectric constant. In the present paper, ε is taken as 8.76 or 2.56. These correspond to the experiments for Si_3N_4 in the millimeter region[11] and polystyrene in the visible region,[7–9] respectively.

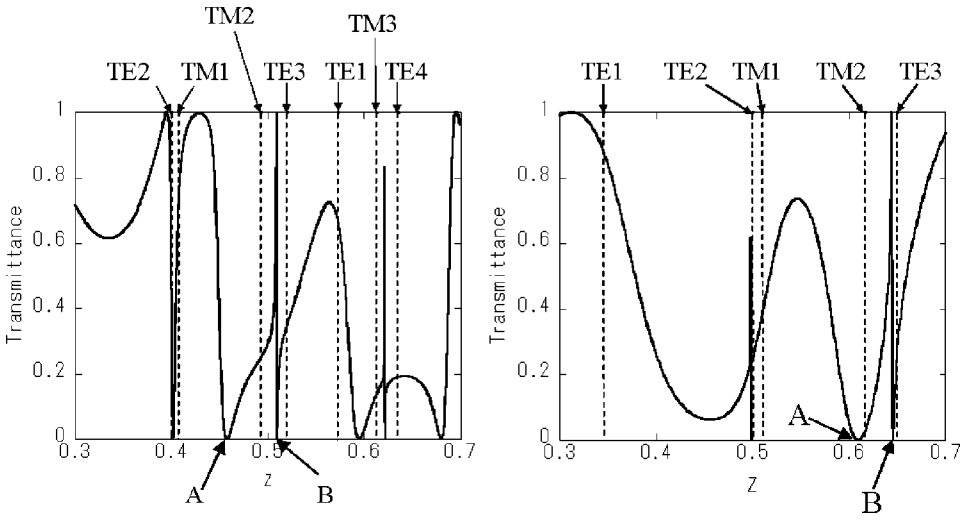

FIG. 2. Transmission spectra for perpendicular incidence. (a) a/d is 0.50 (Ref. 11), (b) a/d is 0.40. ε is 8.76. The vertical and horizontal axes are transmission and normalized frequency $Z = \sqrt{3}d/2\lambda$, respectively. Frequencies corresponding to the single-sphere Mie resonances are shown at the top of this figure. Dips at $Z=0.458$ in (a) and 0.603 in (b) are denoted by A. Dips represented B are excited at $Z=0.510$ and 0.645 in (a) and (b), respectively.

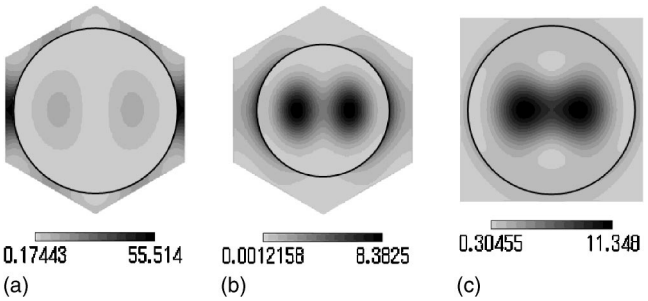

FIG. 3. Distribution of the electric-field intensity in a unit cell (a) at $Z=0.458$ (dip A) in Fig. 2(a), (b) at $Z=0.603$ (dip A) in Fig. 2(b), (c) an isolated sphere at $S=1.788$. The darker region corresponds to the higher field intensity. The height of the sampling plane h is $0.4a$.

The band structure can be obtained from transmission spectra,[6,9–11] since dips in transmission spectra reflect excitation of the eigenstates of the system. Transmission spectra for perpendicular incidence correspond to the Γ point of the band structure. In this paper, we investigate the internal electric-field intensity distribution only for the perpendicular incidence, because discussion at the Γ point is sufficient to understand the origin of each band.

The sampling plane for the field intensity distribution is parallel to the xy plane. The height of the sampling plane h is $0.4a$, as shown in Fig. 1. We show the distribution of the electric-field intensity within a unit cell. Polarized light in the x direction with unit amplitude is incident on the crystals.

In the numerical calculation, the velocity of light in vacuum is taken as $c=1$. The frequency and the wave number of the periodic system are measured in units of dimensionless parameter $Z=\sqrt{3}d/2\lambda$, and those of an isolated sphere is represented by size parameter $S=k_0a$, where λ is the wavelength of the incident light. We take account of $\ell_{\max}=9$, which turns out to give sufficient numerical convergence even for higher dielectric spheres.

First, we discuss the system of $\varepsilon=8.76$. Figure 2(a) is the transmission spectrum for $a/d=0.50$.[11] In addition, that for $a/d=0.40$ is also shown in Fig. 2(b) as a system of weaker interaction between spheres. Sharp dips and broad dips appear alternately in Figs. 2(a) and 2(b). These dips are expected to have different origins. Consequently, we investigate the internal electric field intensity distribution of both dips.

The dip A at $Z=0.458$ in Fig. 2(a) is broad. The dip A in Fig. 2(a) has shifted to $Z=0.603$ in Fig. 2(b). The single sphere Mie resonance of the TM mode for $\ell=2$ (TM2) is at $S=1.788$. This corresponds to the frequencies $Z=0.493$ and 0.616 for the periodic system of $a/d=0.50$ and $a/d=0.40$, respectively. We can guess that the dips A in Figs. 2(a) and 2(b) are related to the Mie resonance of TM2 mode. Therefore, we investigate the internal electric-field intensity distributions at these frequencies.

Figures 3(a) and 3(b) are the internal electric-field intensity distribution at the dips A in Figs. 2(a) and 2(b), respectively. The darker region corresponds to the higher field intensity. While the field is enhanced between spheres in Fig. 3(a), it is localized in the sphere in Fig. 3(b). Figures 3(a) and 3(b) are dominated by x and z components, respectively. In addition, the magnitude of field intensity in Fig. 3(a) is larger than that in Fig. 3(b). However, the distribution inside the sphere in Fig. 3(a) resembles that in Fig. 3(b): the two peaks inside the sphere originate from z component, and those peak values are 8.79. The field distribution of an isolated sphere at the TM2 mode is shown in Fig. 3(c). Figure 3(c) is similar to Fig. 3(b). Consequently, we attribute this eigenstate to the Mie resonance of the TM2 mode. The enhancement between spheres in Fig. 3(a) is considered to be due to the strong interaction in close packed system.

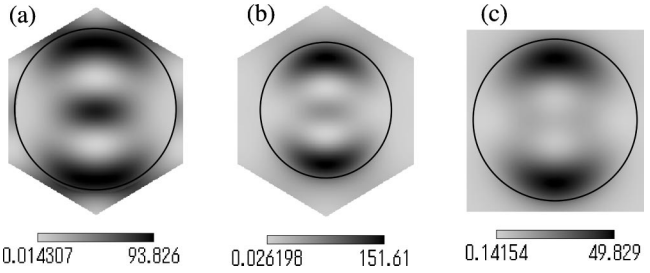

FIG. 4. Distribution of the electric-field intensity (a) at $Z=0.510$ (dip B) in Fig. 2(a), (b) at $Z=0.645$ (dip B) in Fig. 2(b), and (c) an isolated sphere at $S=1.886$.

Next, we discuss the sharp dips. The single sphere Mie resonance of TE mode for $\ell=3$ (TE3) is at $S=1.886$. This corresponds to frequencies $Z=0.520$ and 0.650 for $a/d=0.50$ and $a/d=0.40$, respectively. It is expected that this mode is deeply related with the dips B at $Z=0.510$ in Fig. 2(a) and 0.645 in Fig. 2(b). Therefore, we investigate the internal electric-field intensity distribution at these frequencies.

Figures 4(a) and 4(b) are the distributions of electric field intensity at the dips B in Figs. 2(a) and 2(b), respectively, and Fig. 4(c) is that of an isolated sphere at $S=1.886$. All of Fig. 4 is dominated by the x component. There are two crescent regions at the upper and lower edges. Consequently, the eigenstate of Figs. 4(a) and 4(b) can be attributed to the Mie resonance of the TE3 mode. However, the electric field at the

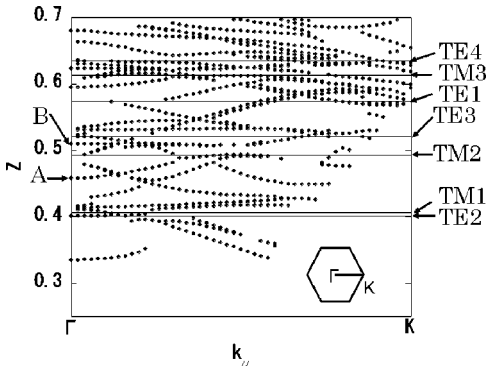

FIG. 5. The p-polarization-active photonic band structure of ΓK direction for $a/d=0.50$. The vertical and horizontal axes are normalized frequency Z and in-plane wave vector, respectively. Frequencies of the single Mie resonances are shown on the right side. The bands corresponding to the dips A and B in Fig. 2(a) are denoted by A and B. The inset is the 2D Brillouin zone.

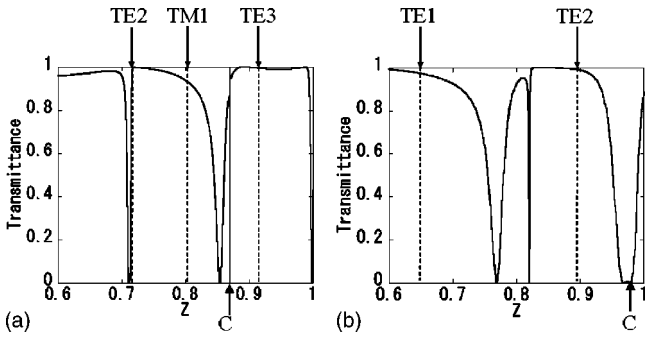

FIG. 6. Transmission spectra for (a) $a/d=0.50$ (Ref. 6), (b) $a/d=0.40$. ε is 2.56. Frequencies at the single-sphere Mie resonance are shown at the top of this figure. Dips at $Z=0.870$ in (a) and $Z=0.979$ in (b) are represented by C.

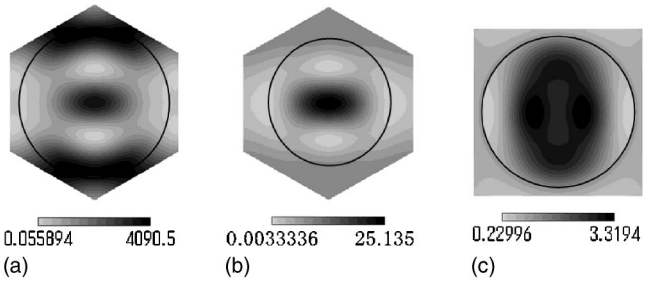

FIG. 7. Distribution of the electric-field intensity (a) at $Z=0.870$ (dip C) in Fig. 6(a), (b) at $Z=0.979$ (dip C) in Fig. 6(b), and (c) an isolated sphere at $S=3.326$.

center is enhanced only in Fig. 4(a). It is considered that this feature is also caused by the interaction between spheres when they are in contact. In general, sharp and broad dips in spectra originate from the Mie resonance of TE and TM modes, respectively.

Figure 5 is the band dispersion of p polarization. The incident light of p polarization is polarized in the xz plane. The band dispersion is obtained from dips in the transmission spectra for oblique incidence. $\mathbf{k}_{\|}$ is scanned along the symmetry axis ΓK of the 2D Brillouin zone. The bandwidths are very narrow; in particular, band B is almost horizontal. Moreover, these flat bands are located around the position of the single sphere Mie resonances. These features lead us to the conclusion that the eigenstate of the monolayer of $\varepsilon=8.76$ is well described by the tight-binding model.

Next, we turn to the case of $\varepsilon=2.56$. We also investigate the internal electric-field intensity distribution at dips in transmission spectra for $a/d=0.50$ and $a/d=0.40$. Figures 6(a) and 6(b) are transmission spectra for $a/d=0.50$ (Ref. 6) and $a/d=0.40$, respectively. There are four dips both in Figs. 6(a) and 6(b). Note that dips at $Z=0.712$ in Fig. 6(a) are almost doubly degenerate. The single sphere Mie resonance of the TE3 mode is at $S=3.326$; this corresponds to $Z=0.917$ for $a/d=0.50$ and $Z=1.146$ for $a/d=0.40$ [not shown in Fig. 6(b)]. This frequency is close to the dip C at $Z=0.870$ in Fig. 6(a). In addition, the dips C in Fig. 6(a) shift to $Z=0.979$ in Fig. 6(b). Consequently, we investigate the field intensity distribution at dips C in Figs. 6(a) and 6(b).

Figures 7(a) and 7(b) are distributions of the field intensity at dip C in Figs. 6(a) and 6(b), respectively, and Fig. 7(c) is that of an isolated sphere at $S=3.326$. All of Fig. 7 is dominated by the x component. Three regions of high intensity in Fig. 7(a) change to a single region at the center of the sphere in Fig. 7(b). Simultaneously, the magnitude of the field intensity decreases drastically. In addition, the field intensity of Fig. 7(c) is much smaller than those of Figs. 7(a) and 7(b), and the shape of distribution is different. Thus, it is not possible to explain the electric-field intensity distribution of the system of $\varepsilon=2.56$ by the tight-binding approximation. In the case of a weaker interaction, i.e., smaller radius of spheres and lower dielectric constant, the frequency of the eigenstate approaches that of free photon.[5,14] In addition, the band structure of this system is essentially obtained by the folding of the dispersion of free photon in the Brillouin zone (see, e.g., Fig. 11 of Ref. 6). Therefore, it is natural to suppose that photons in the system with low dielectric constant behave as free photons.

In this paper, we have extended the vector KKR method to calculate the internal electric field of the monolayer. The scattered field is expanded in terms of the spherical waves, and the internal electric field of spheres is obtained by taking account of the boundary condition at the surface of spheres. From the internal electric-field intensity distribution, we can discuss the origin of the eigenstate of the monolayer. It is found that the eigenstate of the monolayer of $\varepsilon=8.76$ is well described by the tight-binding picture. On the other hand, the internal electric-field intensity distribution of the monolayer of $\varepsilon=2.56$ is very different from that of an isolated sphere, since the electric field can hardly localize within the spheres. Fundamental knowledge on the origin of photonic bands presented in this paper would be valuable in designing various kinds of PhC's.

The authors would like to thank K. Ohtaka, S. Yamaguti, H. T. Miyazaki, and Y. Segawa for useful comments and valuable discussion. This work was supported by a Grant-in-Aid for Scientific Research from the Ministry of Education, Calture, Sports, Science, and Technology.

*Electronic address: KUROKAWA.Yoichi@nims.go.jp

[1] J. D. Joannopoulos, R. D. Meade, and J. N. Winn, *Photonic Crystals* (Princeton University Press, Princeton, 1995).
[2] E. Yablonovitch, Phys. Rev. Lett. **58**, 2059 (1987).
[3] J. D. Joannopoulos, P. R. Villeneuve, and S. Fan, Nature (London) **386**, 143 (1997).
[4] H. Kosaka, T. Kawashima, A. Tomita, M. Notomi, T. Tamamura, T. Sato, and S. Kawakami, Phys. Rev. B **58**, R10 096 (1998).
[5] M. Inoue, Phys. Rev. B **36**, 2852 (1987).
[6] H. Miyazaki and K. Ohtaka, Phys. Rev. B **58**, 6920 (1998).

[7] T. Fujimura, T. Itoh, A. Imada, R. Shimada, T. Koda, N. Chiba, H. Muramatsu, H. Miyazaki, and K. Ohtaka, J. Lumin. **87-89**, 954 (2000).
[8] R. Shimada, Y. Komori, T. Koda, T. Fujimura, T. Itoh, and K. Ohtaka, Mol. Cryst. Liq. Cryst. Sci. Technol., Sect. A **349**, 5 (2000).
[9] H. T. Miyazaki, H. Miyazaki, K. Ohtaka, and T. Sato, J. Appl. Phys. **87**, 7152 (2000).
[10] K. Ohtaka, Y. Suda, S. Nagano, T. Ueta, A. Imada, T. Koda, J. S. Bae, K. Mizuno, S. Yano, and Y. Segawa, Phys. Rev. B **61**, 5267 (2000).
[11] T. Kondo, M. Hangyo, S. Yamaguchi, S. Yano, Y. Segawa, and K. Ohtaka, Phys. Rev. B **66**, 033111 (2002).
[12] N. W. Ashcroft and N. D. Mermin, *Solid State Physics* (Saunders College, Philadelphia, 1976).
[13] G. Mie, Ann. Phys. (Leipzig) **25**, 377 (1908); M. Born and E. Wolf, *Principles of Optics* (Pergamon, Oxford, 1965), p. 633.
[14] T. Ochiai and K. Sakoda, Phys. Rev. B **64**, 045108 (2001).
[15] K. Ohtaka, Phys. Rev. B **19**, 5057 (1979).
[16] K. Ohtaka, J. Phys. C **13**, 667 (1980).
[17] K. Kambe, Z. Naturforsch. A **22A**, 322 (1967).